

Research article

Isolation and characterization of new *Saccharomyces cerevisiae* mutants perturbed in nuclear pore complex assembly

Kathryn J Ryan and Susan R Wentz*

Address: Department of Cell Biology and Physiology, Washington University School of Medicine, St. Louis, MO 63110, USA

E-mail: Kathryn J Ryan - kathryn.ryan@vanderbilt.edu; Susan R Wentz* - susan.wentz@vanderbilt.edu

*Corresponding author

Published: 5 September 2002

Received: 24 July 2002

BMC Genetics 2002, **3**:17

Accepted: 5 September 2002

This article is available from: <http://www.biomedcentral.com/1471-2156/3/17>

© 2002 Ryan and Wentz; licensee BioMed Central Ltd. This article is published in Open Access: verbatim copying and redistribution of this article are permitted in all media for any non-commercial purpose, provided this notice is preserved along with the article's original URL.

Abstract

Background: Nuclear pore complexes (NPCs) are essential for facilitated, directional nuclear transport; however, the mechanism by which ~30 different nucleoporins (nups) are assembled into NPCs is unknown. We combined a genetic strategy in *Saccharomyces cerevisiae* with Green Fluorescence Protein (GFP) technology to identify mutants in NPC structure, assembly, and localization. To identify such mutants, a bank of temperature sensitive strains was generated and examined by fluorescence microscopy for mislocalization of GFP-tagged nups at the non-permissive temperature.

Results: A total of 121 mutant strains were isolated, with most showing GFP-Nic96 and Nup170-GFP mislocalized to discrete, cytoplasmic foci. By electron microscopy, several mutants also displayed an expansion of the endoplasmic reticulum (ER). Complementation analysis identified several mutant groups with defects in components required for ER/Golgi trafficking (*sec13*, *sec23*, *sec27*, and *bet3*). By directed testing, we found that mutant alleles of all COPII components resulted in altered GFP-Nup localization. Finally, at least nine unknown complementation groups were identified that lack secretion defects.

Conclusion: The isolation of *sec* mutants in the screen could reflect a direct role for vesicle fusion or the COPII coat during NPC assembly; however, only those *sec* mutants that altered ER structure affected Nup localization. This suggests that the GFP-Nup mislocalization phenotypes observed in these mutants were the indirect result of overproliferation of the ER and connected outer nuclear envelope. The identification of potentially novel mutants with no secretory defects suggests the distinct GFP-Nup localization defects in other mutants in the collection will provide insights into NPC structure and assembly.

Background

Trafficking between the nuclear and cytoplasmic compartments is mediated by nuclear pore complexes (NPCs) [1,2]. These large, proteinaceous structures are embedded in a nuclear envelope (NE) pore formed by fusion of the inner and outer nuclear membranes. The three dimen-

sional structure of NPCs from both *Xenopus* and budding yeast *Saccharomyces cerevisiae* is characterized by distinct substructures that are arranged with an 8-fold rotational symmetry [3]. Eight spoke-like structures form the central NPC core and are flanked on the cytoplasmic and nuclear sides by ring structures. Fibrils protrude from both the cy-

toplasmic and nuclear rings, with the nuclear fibrils gathered into a basket-like structure by a terminal ring. The global architectures of the yeast and vertebrate NPCs are highly similar, although there may be differences in the core ring structures [4]. Genetic and biochemical studies in yeast have identified ~30 NPC proteins (termed nucleoporins, Nups) that comprise the estimated ~44 MDa structure [5]. Recent proteomic analysis has determined that mammalian NPCs are also comprised of ~30 different proteins [6]; however, the overall size of the vertebrate NPC is predicted to be larger [3,6–8]. Despite their size differences, yeast and vertebrate NPCs are responsible for identical transport reactions, and therefore, both structures are predicted to be functionally equivalent [9].

NPC assembly is likely to be a highly regulated process that coordinates membrane fusion with the coincident assembly of peripheral nucleoporins. Biogenesis of NPCs takes place throughout the cell cycle in all cell types. De novo assembly into intact NEs occurs during cell and nuclear growth to maintain a constant NPC density [10]. In cells undergoing an open mitosis, NPCs are also re-assembled with the formation of the NE at the end of mitosis [11]. The mechanisms controlling membrane fusion during pore formation and the steps for assembly of the distinct NPC substructures have not been fully elucidated. Understanding the molecular pathway of NPC biogenesis will be a critical step in determining the mechanism of NPC function.

Current models for NPC assembly are based on a combination of *in vivo* and *in vitro* studies. Experiments using immuno-fluorescence in vertebrate cells are beginning to order the recruitment and timing of incorporation of individual nucleoporins during post-mitotic re-assembly [12–15]. Additionally, *in vitro* assembly studies with *Xenopus* egg or mitotic cell extracts have revealed several intermediates in NPC assembly and demonstrated a requirement for an intact double nuclear membrane prior to post-mitotic NPC assembly [16–19]. The modular nature of the NPC structure has also suggested that subcomplexes of discrete Nups may initially form and provide building blocks for biogenesis. In fact, Hurt and coworkers have recently demonstrated the *in vitro* assembly of a Nup subcomplex from entirely recombinant proteins [20]. Given the structural and functional similarities between vertebrate and yeast NPCs and the insertion of both into a pre-existing NEs, it is likely that NPC biogenesis occurs via a similar mechanism in all organisms.

We and others have focused on genetic analysis in the budding yeast *S. cerevisiae* to understand the mechanism of NPC biogenesis. This approach has mostly involved reverse genetics wherein mutations in a gene encoding a known nucleoporin are evaluated for NPC structural and

functional changes, and several mutants that induce massive morphological perturbations have been characterized [21–24]. However, the advent of green fluorescence protein (GFP)-based technology has recently allowed forward genetic strategies. Using GFP-tagged NPCs, we designed live cell assays to monitor NPC dynamics and assembly rates [25]. Moreover, to isolate factors required for proper NPC assembly and localization, we developed a novel genetic screening strategy. The approach is based on the ability to express functional GFP-nucleoporin fusions, and the assumption that NPC assembly/mislocalization mutants expressing a GFP-nucleoporin will have distinct fluorescence properties as compared to wild type cells. Our previous studies used fluorescence-activated cell sorting to isolate mutants and identified a *nup57* mutant with diminished incorporation of the GFP-Nup49p at the NPC [26]. As Nup57p and Nup49p directly interact in the NPC structure [27,28], this provided a powerful strategy for pinpointing nearest neighbor interaction requirements. We have now extended this analysis and employed classic temperature sensitive mutant collection with a strain expressing multiple GFP-tagged nucleoporins. This modified approach was designed to isolate mutants that affect global NPC assembly. We report here the complete mutant screen identifying 121 individual mutants that subdivide into at least 11 complementation groups. Further analysis of mutant subgroups has revealed potential mechanisms for both direct and indirect perturbation of NPC assembly and localization, and indicates that this process requires multiple factors

Results

Rationale for a genetic screen to identify temperature sensitive mutants that perturb NPC assembly and localization

Work in our previous studies suggested that GFP-based screening for NPC assembly mutants (designated *npa*) was a powerful approach. This strategy was based on the ability to functionally express GFP-nucleoporin fusions, and the assumption that NPC assembly/mislocalization mutants expressing a GFP-nucleoporin would have distinct fluorescence properties [26]. In wild type yeast cells, fluorescence microscopy localization of proteins at NPCs appears as punctate staining of virtually the entire nuclear rim circumference (see Figure 2). Mutants perturbing GFP-Nup localization could include cells with 1) NPC clusters in NE subregions, 2) mislocalization of the GFP-Nup or aggregated NPC subcomplexes to the cytoplasm or nucleus (due to either a block in new assembly or increased instability of existing NPCs), 3) mislocalization of the GFP-Nup due to indirect perturbation of the ER and NE membrane, or 4) decreased GFP-Nup incorporation followed by turnover resulting in cells with diminished total fluorescence. Given the lack of knowledge about mediators of NPC assembly and localization, we aimed to bias the genetic strategy towards those with global assem-

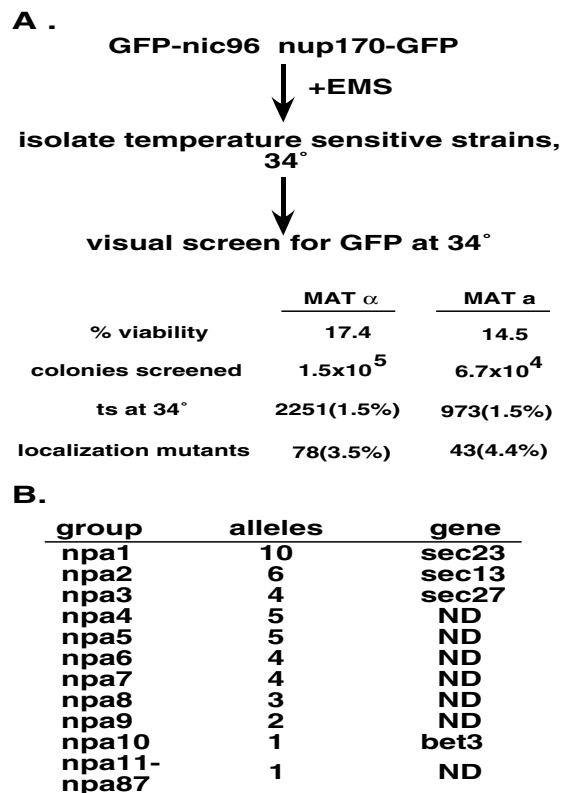


Figure 1
Genetic strategy and isolation of npa mutants. A. Flow chart of the genetic strategy used to isolate NPC assembly mutants (*npa*). B. Results of complementation testing between MATa and MAT α npa mutants. ND, not determined.

bly defects. We predicted that factors required for total NPC biogenesis would be essential, as functional NPCs are absolutely required for nuclear transport. Thus, a primary modification of our original strategy was to generate a bank of temperature sensitive (ts) mutants from a parental strain expressing GFP-Nup(s). Examining the direct GFP-Nup fluorescence of each member of the bank would isolate potential *npa* strains. Second, we sought to preferentially isolate mutants that decrease overall NPC number versus inhibiting the incorporation of the single GFP-Nup. We predicted that co-expression of multiple GFP-Nups that localize to distinct NPC substructures would allow identification of mutants with global defects.

For such a screen, haploid strains expressing chromosomally integrated GFP fusions to both *NIC96* and *NUP170* were generated (see Materials and Methods). *NIC96* is an essential nucleoporin and a member of multiple biochemically distinct NPC subcomplexes [29,30]. *NUP170*, while not essential, is physically and genetically linked to a distinct subset of nucleoporins [31–34]. The rationale for using *NIC96* and *NUP170* are several-fold.

Nic96p and *Nup170p* are two of the most abundant nucleoporins [5,31], the characterized *nic96* and *nup170* mutants do not result in gross morphological NPC perturbations (e.g. NPC clusters, NE herniations, or membrane sealing of NPCs) [23,31,35], and in previous studies GFP-epitope tagging of *Nic96p* or *Nup170p* did not inhibit function [26], our unpublished observations]. Finally, the encoded proteins are associated with distinct NPC subcomplexes [2], and we speculated that true mislocalization mutants would require disruption of both sets of subcomplexes and more likely reflect defects in global NPC structure and assembly.

In the doubly tagged *GFP-nic96 nup170-GFP* strains, both GFP-*Nic96p* and *Nup170p-GFP* were targeted to the NE and showed punctate rim-staining characteristic of NPC localization (Figure 2). However, the combination of these two protein fusions in a haploid strain resulted in a ts phenotype at 37°. The ts phenotype was not, however, accompanied by mislocalization of GFP-Nups after growth for 6 hours at 37°. The strain was viable at 34° and doubling times were similar to wild type cells at 34°. We predicted this sensitized background might further bias the screen toward mutations that perturb NPC structure.

Isolation of npa mutants

Wild type *GFP-nic96 nup170-GFP* haploid strains were mutagenized to generate a bank of ts mutant strains (Figure 1A; see Materials and Methods). To identify mutants from this bank, individual ts strains were visually screened for GFP-Nup localization by fluorescence microscopy after shifting cultures to the non-permissive temperature (34°) for 4–6 hours. A total of 121 individual *npa* strains were identified in which the GFP-Nup signal was altered. The mutant phenotypes were largely penetrant with all cells from a mutant strain responding identically. None of the cells in a mutant population had retained a completely normal appearance when assayed. Although most mutants had relatively normal growth rates at the permissive temperature, many showed signs of cell stress as indicated by large cell and vacuole size (Figure 2, DIC panels). While our previous screen identified mutants with either a diminished GFP signal (dim mutants) or NPC clusters [26], very few of the mutants isolated in this screen (5/121) showed a temperature dependent decrease in fluorescence intensity (Figure 2, compare panels A and C to M and O). Instead, most mutants lost the exclusive, punctate nuclear rim localization, the GFP-Nups were present in areas distinct from the NE and often in discrete foci (Figure 2, panels G and K). The majority showed wild type GFP localization at the permissive growth temperature (23°); however some did show a weak mislocalization phenotype at 23° that was significantly enhanced when the cells were shifted to growth at 34° (Figure 2, panels E and G). Intriguingly, some of the mutants also had an apparent in-

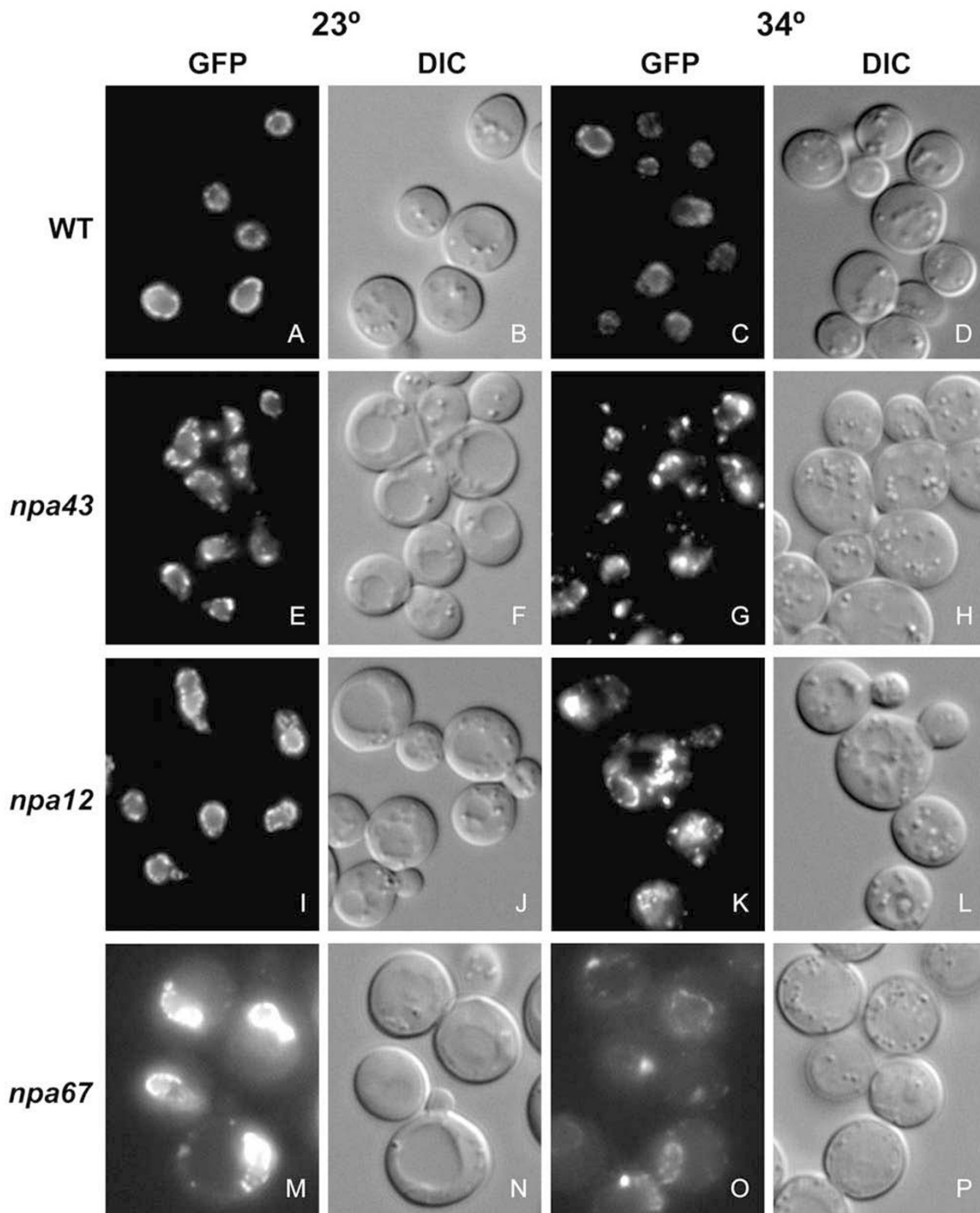


Figure 2
GFP-Nup localization in *npa* mutants. Isolated assembly mutant strains along with the parental strain were grown to early log phase at 23° then shifted to the non-permissive temperature of 34° for 4 hours. Localization of GFP-Nic96p and Nup170p-GFP was visualized by direct fluorescence microscopy, and all GFP images were collected for the same exposure time. WT cells (SWY2089) maintain a characteristic punctate nuclear rim staining, indicative of NPC localization, throughout the temperature shift. In contrast, the mutants display various localization phenotypes including NPC clusters (*npa43*, G), cytoplasmic and nuclear foci (*npa12*, K), and a diminished GFP-Nup signal (*npa67*, O). Note that while Nup-GFP localization is already affected at 23° in *npa43* (E) and *npa67* (M), the phenotype is exacerbated at 34° (G and O).

crease in GFP intensity (Figure 2, panel M). We speculate that this is due to changes in nearest neighbor interactions such as those observed with GFP-Nup82p in a *nup57* mutant [26].

To determine the number of independent mutant genes isolated, complementation analysis of the *ts* phenotype was performed. Based on pairwise crosses of mutants with opposite mating type, only one-third (37/121) of the mutants were initially catalogued into 8 different complementation groups (Figure 1B). The remaining two-thirds (84/121) of the mutants could not be assigned to a complementation group. Subsequent backcrossing and isolation of opposite mating type strains for some of the mutants allowed definition of an additional complementation group. However, the majority of the mutants were apparently unique with only single mutant alleles isolated. This suggested that the screen was not saturating. Overall, the large number of independent *npa* mutants (potentially 87) was surprising and suggested that a number of distinct proteins can affect NPC assembly and localization.

Nup localization analysis in *npa* strains

To investigate the effects on NPCs more directly, we first targeted members of the largest independent complementation groups for analysis. The mutants displaying the strongest GFP-Nup mislocalization phenotypes were backcrossed. In each case, the GFP-Nup phenotype segregated 2:2 and was genetically linked to the *ts* phenotype indicating a single mutation was responsible for both. Interestingly, mutant alleles in the two largest complementation groups showed a similar pattern of GFP-Nup mislocalization. To investigate NPC structure more closely in *npa1-1* and *npa2-1* mutants, logarithmically growing cultures were shifted to the non-permissive temperature and assayed for GFP-Nup localization by direct fluorescence microscopy at various times after the shift. The parental strain, SWY2089, maintained wild-type nuclear rim localization during growth at 34° (Figure 2, panels A-D). In contrast, both mutants showed a temperature dependent mislocalization of GFP-Nic96p and Nup170p-GFP over a four hour time course (Figure 3). Both *npa1-1* and *npa2-1* cells ceased growing after 3–4 hours at the non-permissive temperature. During this time they completed 1 or 2 cell divisions. Previous studies of *nic96* mutants have shown that cells may undergo 2 to 3 cell divisions with no apparent NPC assembly. Thus, the more rapid onset of growth arrest in *npa1* and *npa2* mutants suggested that the *ts* phenotype was not caused exclusively by a decrease in NPC number and nucleo-cytoplasmic transport capacity [23,35] and may be due to other cellular effects. Other members of the *npa1* and *npa2* complementation groups showed similar phenotypes (data not shown). In addition, Western analysis showed no decrease in GFP-

Nup protein levels in arrested *npa1-1* cells indicating GFP protein stability was not affected (data not shown).

One of our original predictions was that labeling multiple Nups with GFP would identify mutants with defects in the formation of the entire NPC structure. To determine if additional, non-GFP tagged Nups were mislocalized in these cells, we used indirect immunofluorescence (IF) microscopy with antibodies directed against either Nup116p or Pom152p. Like GFP-Nic96p and Nup170p-GFP, the localization of Nup116p and Pom152p changed from a punctate, nuclear rim staining to cytoplasmic foci when shifted to the non-permissive temperature (data not shown).

Ultrastructural analysis of mutants by thin section electron microscopy

Thin-section electron microscopy (TEM) was conducted to evaluate NPC, NE and cellular morphology. After staining with osmium tetroxide and uranyl acetate, NPCs in wild-type/parental cells were represented by electron dense structures spanning the pore (Figure 4). In *npa1-1* and *npa2-1* cells, several distinct perturbations were noted. At the permissive temperature, *npa1-1* cells showed nuclear invaginations. In Figure 4E, a single cell cross-section showed multiple layers of NE containing NPCs. However, the GFP-Nup localization appeared normal in these cells at 23° (Figure 3). After shifting to the non-permissive temperature of 34° for 4 hours, there was a dramatic change in structural morphology in both *npa1-1* and *npa2-1* mutants. Most striking was the overproliferation of outer nuclear/endoplasmic reticulum (ER) membranes. This proliferation was often observed originating from the nucleus and resulted in a regular honeycomb-like array of ~100 nm diameter tubules (Figure 4C and 4F). Although it was not always possible to definitively identify a nucleus in each section (Figure 4F, for example), NPCs were present in the envelope juxtaposed to the nucleus despite the expanded membranes (Figure 4C and 4D). Electron dense structures resembling NPCs were also embedded in membranes distinct from the nucleus/NE (Figure 4F). This most likely corresponded with the cytoplasmic foci observed by fluorescence. We did not observe any evidence of cytoplasmic annulate lamellae formation, although nuclear invaginations sometimes resulted in juxtaposed double membranes containing NPCs (Figure 4F). There were also no structures resembling the intra-nuclear annulate lamellae observed in some *nup* mutants [24,36]. Samples analyzed by TEM over a time course after shift to 34° showed that the membrane proliferation paralleled the GFP-Nup mislocalization seen by fluorescence microscopy (data not shown). This further suggested that the GFP-Nup mislocalization and TEM membrane proliferation were the consequence of the same process.

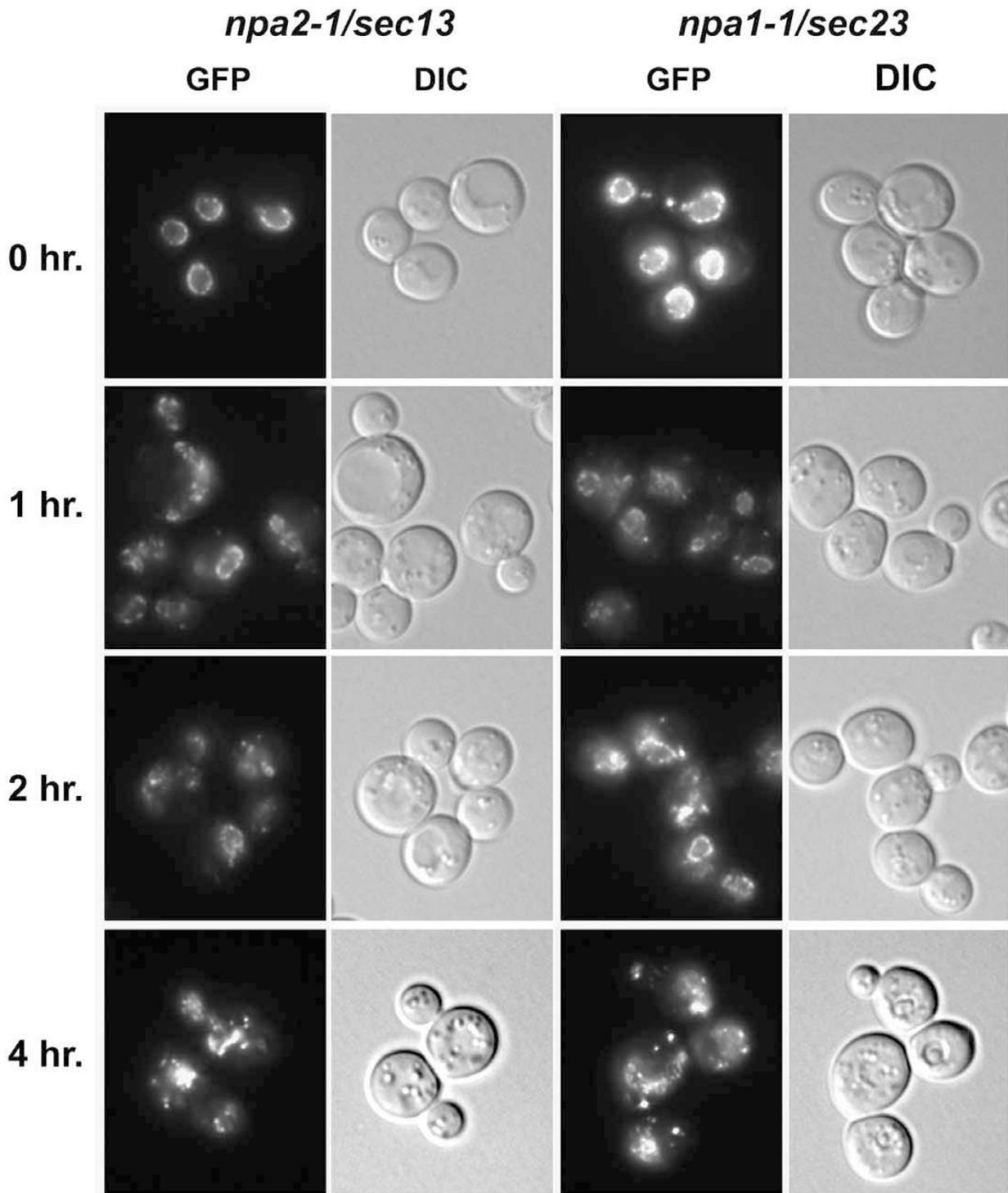


Figure 3
GFP-Nup localization in *npa2/sec13* and *npa1/sec23* mutants. Isolated mutant strains *npa2-1/sec13-G176R* and *npa1-1/sec23-S383L* were grown to early log phase at 23°, and then shifted to 34° for the indicated times. Localization of GFP-Nic96p and Nup170p-GFP was visualized by direct fluorescence microscopy. All GFP fluorescence images were taken for the same exposure time.

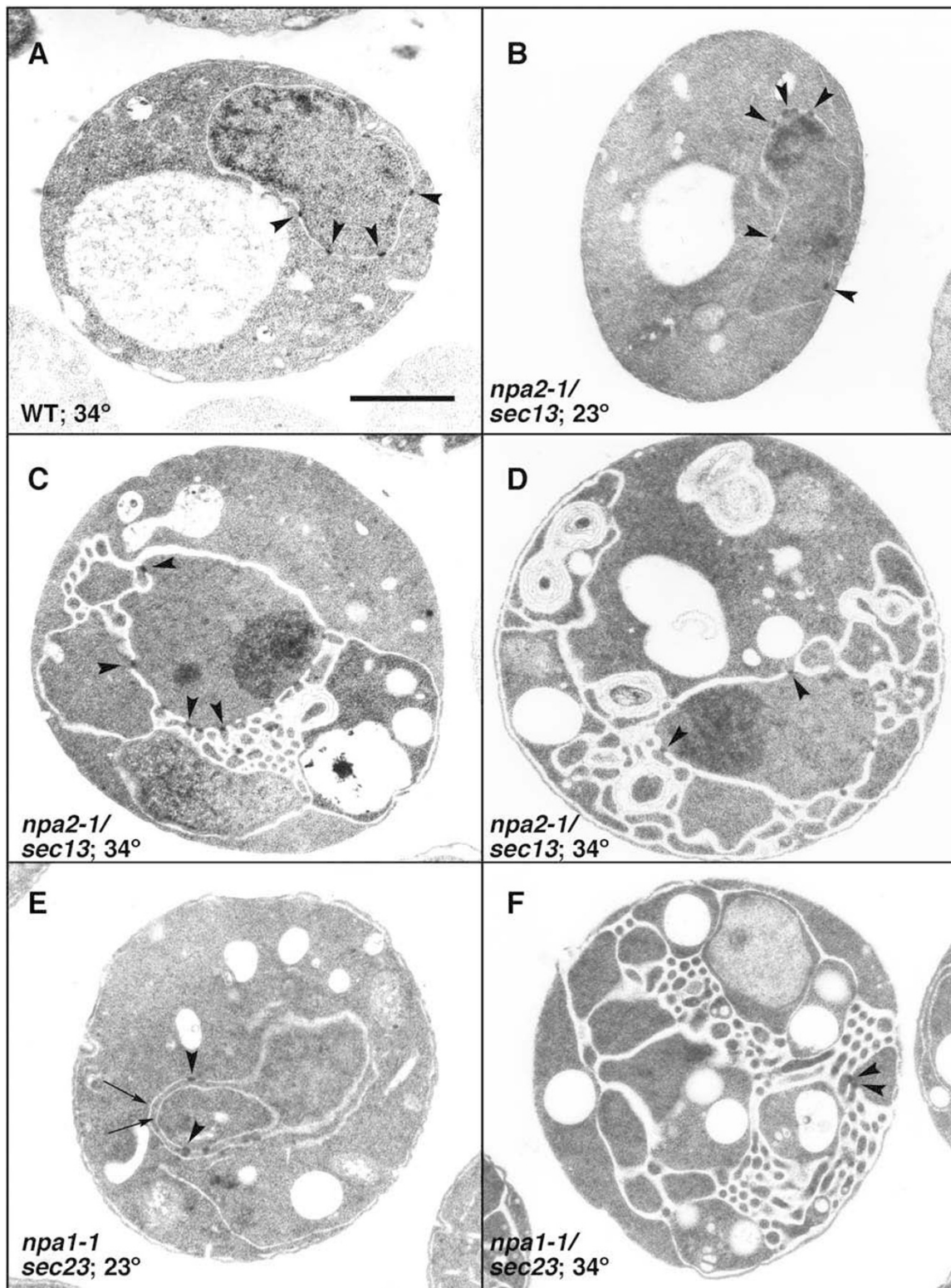


Figure 4
Thin section electron micrographs of *npa2/sec13* and *npa1/sec23* mutants. Cells growing in early log phase were shifted to the permissive (B and E) or the non-permissive (A, C, D and F) temperature for 4 hours before processing for TEM. Arrowheads denote NPC structures. The arrows in E show multiple layers of NE. Bar equals 1 μ m.

Identification of mutants

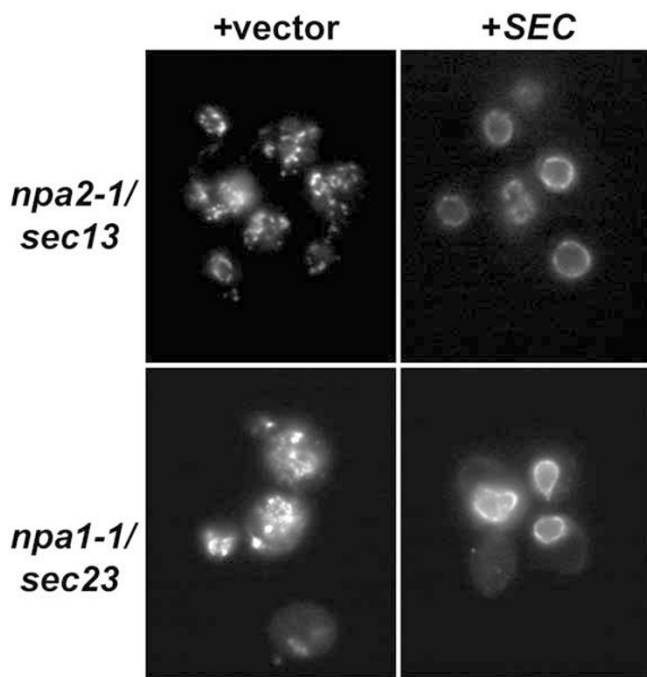


Figure 5
Rescue of GFP-Nup localization in mutants by transformation with SEC13 or SEC23. Mutants *npa2-1/sec13-G176R* and *npa1-1/sec23-S383L* were transformed with an empty pRS315 vector (+vector), the vector containing SEC13 (*npa2-1*), or the vector containing SEC23 (*npa1-1*) (+SEC). Strains were grown for 4 hours at 34°C and GFP-Nup localization visualized as in Figures 2 and 3.

To identify the mutated genes, a yeast genomic library was screened for complementation of the recessive ts phenotypes of representative mutants. Multiple genomic inserts capable of rescuing the ts growth defect were isolated for each strain. Sequencing and comparison to the *Saccharomyces* Genome Database identified a minimal overlapping region on chromosome XII for the *npa2-1* complementing plasmids, and on chromosome XVI in the *npa1-1* complementing plasmids. Both regions contained multiple open reading frames; however, we focused immediately on a single gene for each mutant, SEC13 for *npa2-1* and SEC23 for *npa1-1*. SEC13 was first identified in a screen for secretory mutants and encodes a protein of the COPII coat, which is required for vesicle budding from the ER [37–39]. More recently, it has been shown that a fraction of the total cellular Sec13p co-fractionates with NPCs in a distinct subcomplex with Nup84p, Nup85p, Nup120p, Nup145Cp and Seh1p [40,41]. SEC23 was also identified in a screen for secretory mutants, and it, too, is a component of the COPII coat [37–39]. Co-purification of Sec23p with intact NPCs has not been reported [5]; however,

Sec23p was recently isolated in Nup42p and Nup116p affinity chromatography strategies [42]. Expression constructs containing only SEC13 or SEC23 were transformed into the mutant strains and assayed for their ability to rescue growth at the non-permissive temperature. Both minimal constructs only restored growth of their respective strain (data not shown). Importantly, the GFP-Nup localization phenotype was also complemented (Figure 5).

The ability of SEC13 and SEC23 to complement the mutants strongly suggested that mutations in these genes were responsible for the observed phenotypes. However, it was still a formal possibility that the overexpression of these genes from a low copy plasmid was sufficient for complementation. To eliminate this possibility, genomic DNA from each of the mutants was used as a template in PCR reactions to generate expression plasmids (see Materials and Methods). Sequencing of the *npa2-1/sec13* allele identified a single G to A transition that changed a Gly to Arg at position 176 in the protein. To test if this mutation was necessary and sufficient for the observed phenotype, the mutant plasmid was transformed into the original *npa2-1* mutant and a *sec13Δ* covered by pSEC13 URA3. Expression of psec13-G176R complemented the otherwise lethal *sec13Δ* at 23°C; however, its expression was not sufficient to restore growth at the non-permissive temperature to either the isolated *npa2-1* mutant or *sec13Δ* (data not shown). DNA sequencing analysis showed that the *npa1-1/sec23* mutant was identical to the well-characterized *sec23-1* (S383L) mutant allele [43].

The accumulation of non-secreted protein in mutants defective in ER to Golgi transport leads to proliferation of the ER [37,44]. The membrane proliferation seen by TEM in *npa1-1/sec23* and *npa2-1/sec13* cells (Figure 4) and the coincident mislocalization of Nups (Figure 3 and data not shown) prompted us to test if Nups were accumulating at the ER. Logarithmically growing cultures of *npa1-1/sec23* and *npa2-1/sec13* were shifted to the non-permissive temperature as before and then fixed and processed for IF with polyclonal antibodies against Kar2p to visualize the ER [45]. The monoclonal antibody mAb414, which recognizes a subset of Nups distinct from Nic96p and Nup170p [46], was also used because the GFP fluorescence of the GFP-Nups was more sensitive to fixation when the GFP-Nups were mislocalized than when they remained at the nuclear rim (unpublished observation). In *npa2-1/sec13* cells, the ER became punctate and formed discrete foci at later time points (Figure 6A). In contrast, *npa1-1/sec23* cells rapidly accumulate an interconnected ER network (Figure 6B). Expansion and changes in ER morphology were observed as early as one hour after the temperature shift, and continued to increase in magnitude over the four hour time course (Figure 6). Although the localization patterns at late time points after temperature shifting

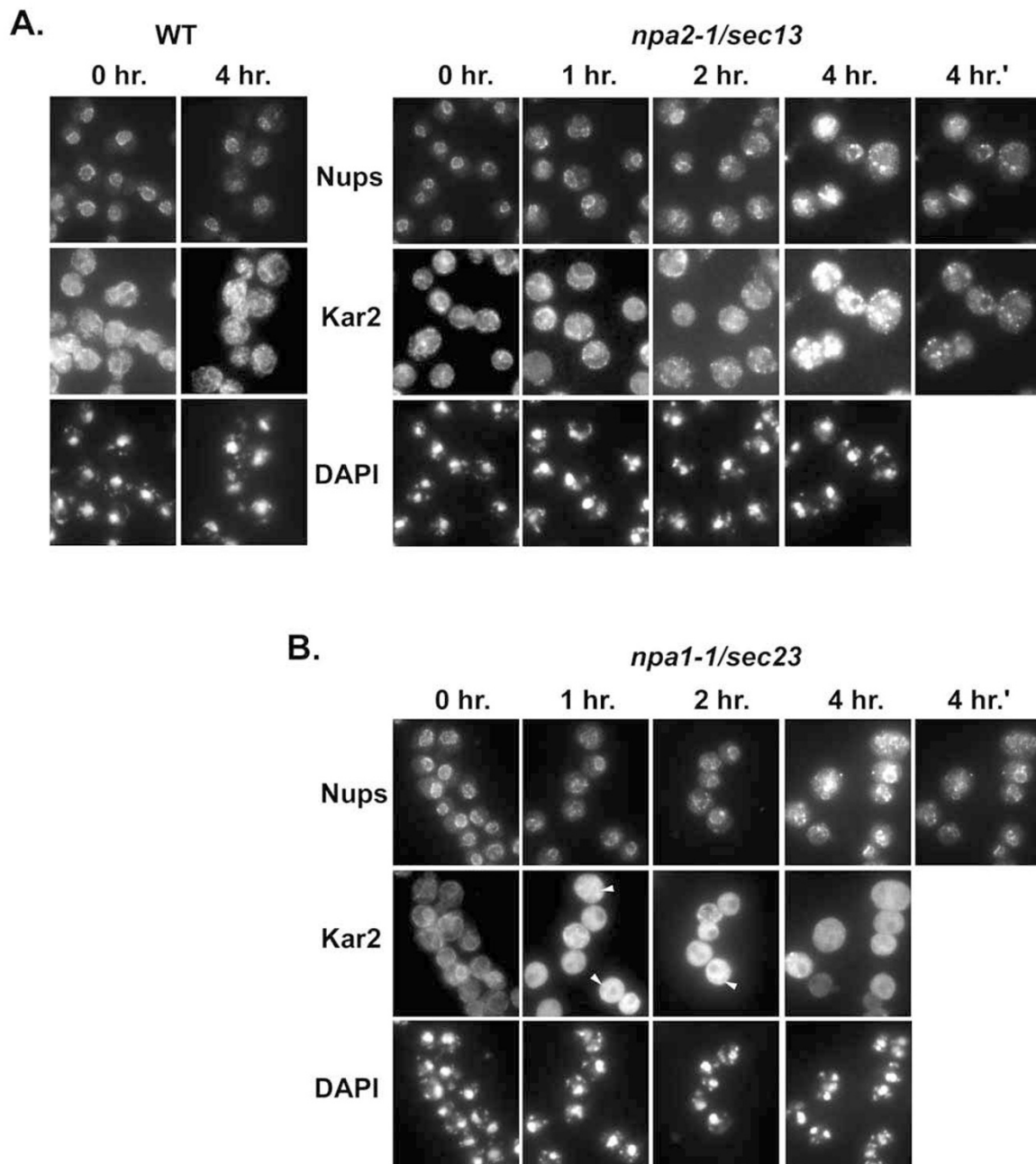


Figure 6
Comparison of nucleoporin localization with an ER luminal protein, Kar2, in *npa2-1/sec13* and *npa1-1/sec23* cells. Cells were shifted to 34° for the indicated times and processed for double-label IF with the monoclonal antibody mAb414 (Nups) and the rabbit polyclonal anti-Kar2 antibody. As the GFP-Nups were still present in these cells, the Nup signal resulted from a combination of GFP-Nic96, Nup170-GFP and the Nups recognized by mAb414. **A.** Wild-type (WT) and *npa2-1/sec13* panels are shown where the 0, 1, 2, and 4 hr. time points are exposed for the same time. The 4 hr.' panels show the same cell field as 4 hr. with decreased exposure times. **B.** Panels showing anti-Nup signal in *npa1-1/sec23* cells were collected for the same exposure times as in **A.** Kar2 exposure times are one quarter of those in **A.**, as the signal was brighter in these cells. Arrowheads denote cells in which the expanded ER network is most evident.

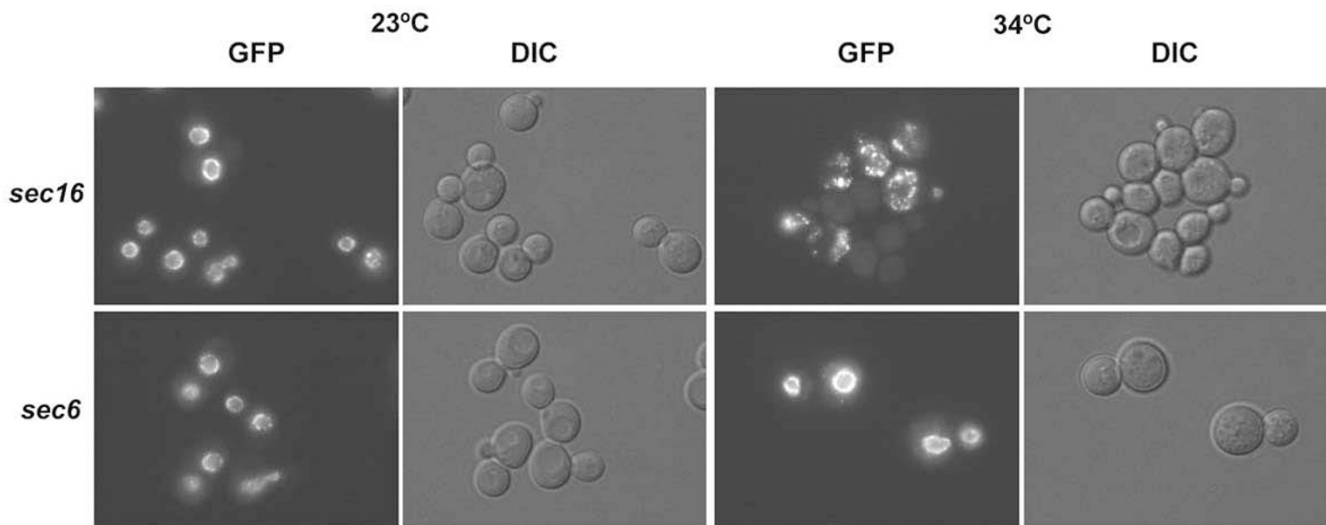


Figure 7
GFP-Nup localization in *sec16* and *sec6* mutants. Localization of GFP-Nic96p and Nup170-GFP in *sec16-2* or *sec6-4* mutant strains was analyzed after growth at 23° or after shifting to growth at 34° for 4 hours. Direct fluorescent signal was monitored.

were similar, the localizations of the ER protein Kar2p and the Nups were not overlapping.

Testing other COPII coat and secretory pathway components for *npa* groups

The screen for NPC assembly/mislocalization mutants identified two genes that are part of the COPII coat, *SEC13* and *SEC23*. To test if other members of the COPII coat complex were isolated in the screen, conditional alleles in *SEC16*, *SEC24*, *SEC31*, *SAR1*, and *SEC12* were kindly provided by other investigators, and tested directly for their effect on NPC localization. The first four genes encode proteins, which along with Sec13p and Sec23p, form the coat while Sec12p is required to recruit and activate Sar1p on the ER for coat assembly [39]. Complementation analysis between these mutants and those isolated in the screen failed to identify any of these. However, when the genes encoding GFP-tagged Nups were crossed into these mutant backgrounds, all displayed GFP-Nup mislocalization under non-permissive conditions (Figure 7 and data not shown). The pattern of mislocalization in each case was similar to that observed in the isolated *sec13* and *sec23* mutants.

Our continued efforts focused on cloning additional *npa* mutants by library complementation. This identified two more genes required for trafficking between the ER and Golgi. A genomic fragment containing *BET3* complemented the ts phenotype of *npa10*, and *npa3-1* was rescued by a library plasmid only when it contained full length *SEC27* (see Materials and Methods). Bet3p is part of a complex that binds to COPII derived vesicles and is re-

quired for vesicle targeting [47,48]. Sec27p is a component of the COPI coat and required for Golgi to ER transport [49,50]. Like *SEC23* and *SEC13* mutants, others have reported that mutants in *BET3* and *SEC27* result in an over-proliferation of ER membranes [49,51].

To determine if the overlap between *npa* mutants and the secretory pathway was restricted to gene products affecting the ER, the *sec6-4* mutant perturbing Golgi to plasma membrane transport [52] was crossed into the *GFP-nic96 nup170-GFP* strain. After 4 hours at 34°, the same conditions that cause GFP-Nup mislocalization in the other assayed *sec* mutants, the GFP-Nups in *sec6-4* remained localized to the NPC in the characteristic, punctate NE rim pattern (Figure 7).

Novel *npa* groups lack secretion defects

The initial isolation of multiple *sec* mutants from our screen that was designed to isolate mutants in NPC assembly and localization raised the question of whether any of the mutants were specific for defects in NPC assembly/structure. To pinpoint mutants that lacked secretion defects, we assayed each mutant from the collection for the ability to secrete the enzyme invertase in response to low glucose. Logarithmically growing cells were transferred to low glucose media and incubated at the non-permissive temperature of 34° for 2.5 hours. When invertase activity from individual mutants was normalized to the activity of the parental strains, a range of relative activities were observed (Figure 8). With the exception of *npa1-3* and *npa1-7*, the *sec23* (*npa1*), *sec13* (*npa2*), and *bet3* (*npa10*) mutants had less than 50% of wild-type invertase activity

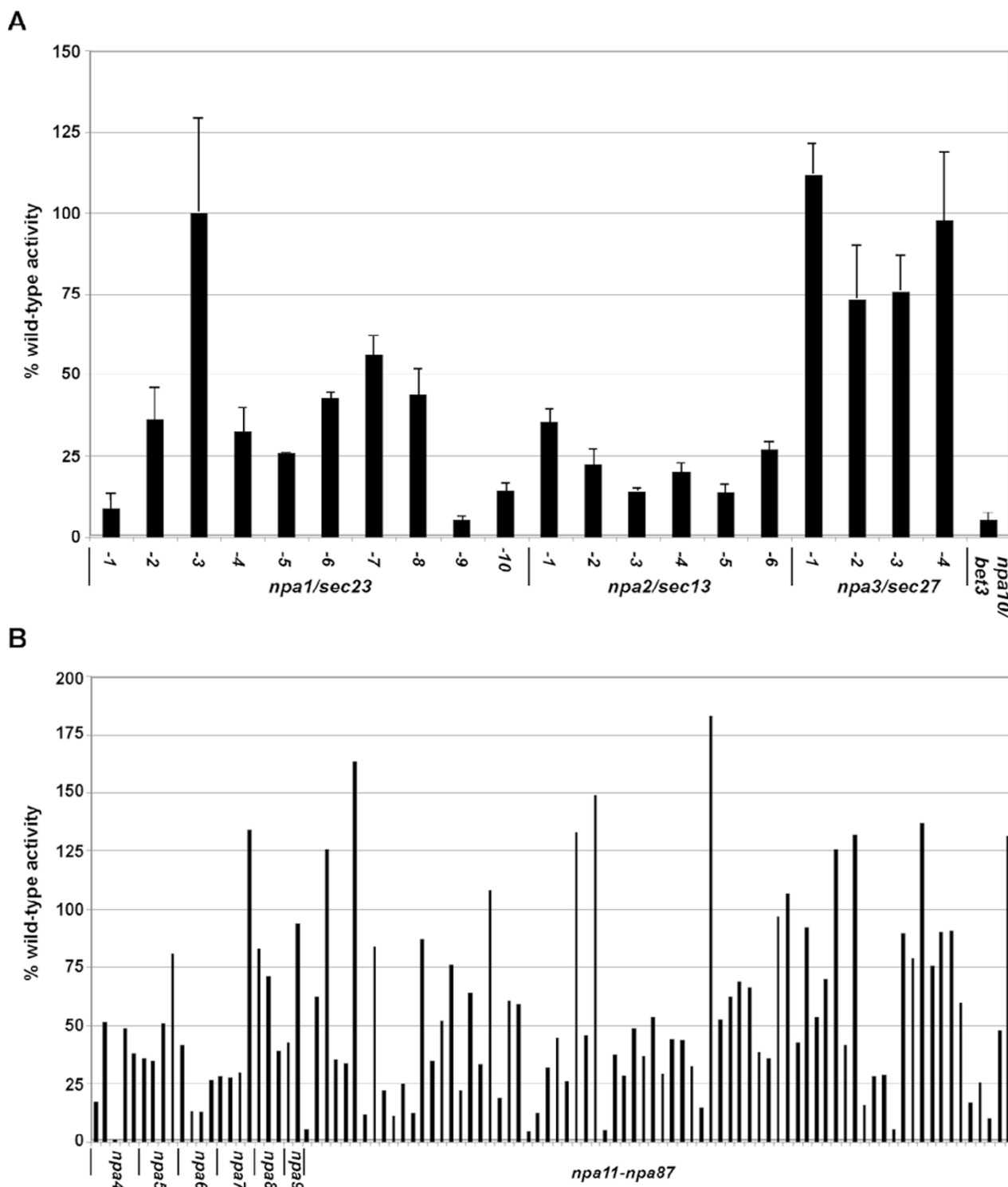


Figure 8
Secreted invertase activity of *npa* mutants. The ability of mutants to secrete the enzyme invertase at the non-permissive temperature (34°) in response to low glucose was determined. Absolute values were normalized to the wild-type control assayed at the same time and plotted as % wild-type activity. **A.** The average % activity and standard deviation of *npa* mutants in the secretory pathway. **B.** Invertase activity from 96 of the remaining 100 uncharacterized *npa* mutants was assayed. In strains assayed multiple times (15/96), the average activity from independent assays is presented.

(Figure 8A). The *npa3/sec27* mutants displayed near wild-type invertase activity indicating that forward trafficking through the ER was not significantly disrupted. This is consistent with secretion results reported for other *sec27* alleles [49,53]. It is important to note that despite the lack of secretion defect, the *npa1-3/sec23*, *npa1-7/sec23*, and *npa3-1/sec27* mutants each had perturbations in ER structure similar to those of *npa1-1* and *npa2-1* (data not shown). The *npa1-3/sec23* and *npa1-7/sec23* mutants may be unique alleles that preferentially affect NPC assembly versus secretion. For the unidentified, potentially novel, mutants, approximately 60% (56/96) had less than half of wild-type invertase activity. This suggests secretion may be impaired in these mutants. Alternatively, these mutants may have defects along the pathway leading to transcriptional up-regulation of invertase (*SUC2*) in response to low glucose [54]. Most importantly, 25% (25/96) of the mutants had at least 75% or greater of wild-type activity (Figure 8B). The lack of secretion defects in some of the mutants indicates that non-nucleoporins are being trafficked properly when Nups are mislocalized.

Discussion

We have used a genetic strategy to identify factors required for proper NPC biogenesis. By creating a bank of ts mutants in a doubly tagged *GFP-nic96 nup170-GFP S. cerevisiae* strain and individually screening the mutants at the non-permissive temperature, we identified 121 ts mutant strains which fail to correctly localize the GFP-Nups at NPCs and/or the NE rim. In addition to the mislocalization of GFP-Nic96p and Nup170p-GFP, Nup116p, Pom152p and Nups recognized by mAb414 were also perturbed in the mutants characterized to date. These Nups are localized throughout the NPC structure [1] and indicate a global defect in NPC assembly/structure. Complementation analysis indicated the mutants were all recessive and fell into at least 11 groups. In comparison to our previous genetic screen with a strain expressing only GFP-Nup49p [26], these results suggest that increasing the number of GFP-Nups as reporters for NPC integrity effectively increases the likelihood of obtaining a panel of mutants defective in global NPC assembly, stability, and localization.

Based on the GFP-Nup localization and genetic analysis, a range of mutant phenotypes and complementation groups were catalogued. Several of the complementation groups contained multiple independent alleles (*npa1-9*), and within a single complementation group the strengths of the defects were varied. However, there was only one allele for the majority of the complementation groups, representing potentially *npa10-87*. This suggests that the mutagenesis was not saturating, and it is likely that mutations in additional genes that function in NPC biogenesis would be isolated by repeated application of this screen-

ing strategy. In addition, the large number of potential total groups may reflect roles for many factors in proper NE/nuclear morphology and NPC biogenesis. We have identified about 30% of the groups by complementation-based cloning. The results thus far indicate the screen is specifically enriched for NE/NPC specific effects versus nonspecific mutants that may affect GFP-Nup protein stability or levels (polymerases, transcription/translation factors, chaperones) (this report and unpublished results). The ts defects in individual *npa* mutants may represent failures in assembly, changes in NPC localization, or perturbations in the stability of pre-existing NPCs.

Here we focused on characterizing the largest complementation groups. The two largest were allelic with *SEC23* and *SEC13*, genes encoding known mediators of vesicular trafficking between the ER and Golgi [39]. The GFP-Nup mislocalization defects in the *sec23* (*npa1*) and *sec13* (*npa2*) mutants correlated with distinct ER membrane perturbations. We also identified *npa3* as *sec27* and *npa10* as *bet3*. Taken together, the recovery of a large number of *npa* mutants that encode components of the ER-Golgi secretory pathway indicate that this is a "hot spot" for mutations that cause perturbations in GFP-Nup localization.

Extensive and elegant studies have documented distinct changes in membrane morphology in mutants with arrest points in the secretory pathway. Three morphological classes include *sec* mutants with extended networks of ER membrane, those with accumulated Golgi, and a third with accumulated 80–100 nm secretory vesicles [37]. The morphological perturbations directly correlate with distinct secretory pathway blocks: ER-Golgi, intra-Golgi, and Golgi-plasma membrane [44]. A recent study in *S. pombe* has also shown that *sec* mutants can affect NE and cell cycle progression [55]. In addition to *sec13*, our screen also identified mutant alleles of *SEC23*, *SEC27* and *BET3*. The mislocalization of GFP-Nups in *sec13* and *sec23* mutants was coincident with the formation of extensive honeycomb networks of ER. Interestingly, we found by direct testing that mutant alleles corresponding to the genes for all known COPII coat components resulted in altered GFP-Nup localization. Based on reports from others, all of these mutants have an over-proliferation of ER membranes [37,44,49,51,56–59]. However, over the same time course, our direct testing of one *sec* mutant with a defect in a later secretion step did not show perturbations (e.g. the *sec6-4* mutant that accumulates secretory vesicles [37] did not result in GFP-Nup mislocalization). Additionally, *sec* mutants with no apparent defect in invertase secretion (*npa1-3/sec23*, *npa1-7/sec23*, and *npa3-1/sec27*) had both perturbations in ER structure and Nup localization. This suggests that mutants which disrupt the ER will affect Nup localization and likely NPC assembly/structure.

Table 1: Yeast Strains

Strain	Genotype	Source
SWY519	<i>MATα ura3-1 his3-11,15 trp1-1 leu2-3,112 can1-100 ade2-1::ADE2:ura3</i>	Bucci and Wente, 1997
SWY1695	<i>MATα ura3-1 his3-11,15 trp1-1 leu2-3,112 can1-100 ade2-1::ADE2:ura3 GFP-nic96:HIS3</i>	Bucci and Wente, 1998
SWY2089	<i>MATα lys2 ura3-1 his3-11,15 leu2-3,112 can1-100 ade2-1::ADE2:ura3 GFP-nic96:HIS3 nup170-GFP:URA3</i>	this study
SWY2090	<i>MATα ura3-1 his3-11,15 trp1-1 leu2-3,112 can1-100 ade2-1::ADE2:ura3 GFP-nic96:HIS3 nup170-GFP:URA3</i>	this study
SWY2324	<i>MATα sec13-G176R (npa2-1) lys2 ura3-1 his3-11,15 leu2-3,112 can1-100 ade2-1::ADE2:ura3 GFP-nic96:HIS3 nup170-GFP:URA3</i>	backcross of <i>npa2-1</i> × SWY2090
SWY2325	<i>MATα sec23-S383L (npa1-1) lys2 ura3-1 his3-11,15 leu2-3,112 can1-100 ade2-1::ADE2:ura3 GFP-nic96:HIS3 nup170-GFP:URA3</i>	backcross of <i>npa1-1</i> × SWY2090
SWY2326	<i>MATα sec6-4 lys2 ura3-1 his3-11,15 leu2-3,112 can1-100 ade2-1::ADE2:ura3 GFP-nic96:HIS3 nup170-GFP:URA3</i>	haploid from SWY2089 × NY17
SWY2327	<i>MATα sec12-4 lys2 ura3-1 his3-11,15 leu2-3,112 can1-100 ade2-1::ADE2:ura3 GFP-nic96:HIS3 nup170-GFP:URA3</i>	haploid from SWY2090 × CKY39
SWY2328	<i>MATα sec16-2 ura3-1 his3-11,15 leu2-3,112 can1-100 ade2-1::ADE2:ura3 GFP-nic96:HIS3 nup170-GFP:URA3</i>	haploid from SWY2089 × RSY268
SWY2329	<i>MATα sar1::URA3 ura3-1 his3-11,15 trp1-1 leu2-3,112 can1-100 ade2-1::ADE2:ura3 GFP-nic96:HIS3 nup170-GFP:URA3 p[GAL1-SAR1 LEU2]</i>	haploid from SWY2090 × ANY27
SWY2330	<i>MATα sec31-1 ura3-1 his3-11,15 leu2-3,112 can1-100 ade2-1::ADE2:ura3 GFP-nic96:HIS3 nup170-GFP:URA3</i>	haploid from SWY2090 × RSY1004
SWY2331	<i>MATα sec24 ura3-1 his3-11,15 trp1-1 leu2-3,112 can1-100 ade2-1::ADE2:ura3 GFP-nic96:HIS3 nup170-GFP:URA3</i>	haploid from SWY2090 × CKY496
SWY2332	<i>MATα sec27(np3-1) ura3-1 his3-11,15 leu2-3,112 can1-100 ade2-1::ADE2:ura3 GFP-nic96:HIS3 nup170-GFP:URA3</i>	backcross of <i>npa3-1</i> × SWY202089
SWY2333	<i>MATα bet3(np10) ura3-1 his3-11,15 trp1-1 leu2-3,112 can1-100 ade2-1::ADE2:ura3 GFP-nic96:HIS3 nup170-GFP:URA3</i>	backcross of <i>npa10</i> × SWY2089
SWY2334	<i>MATα np4312 lys2 ura3-1 his3-11,15 leu2-3,112 can1-100 ade2-1::ADE2:ura3 GFP-nic96:HIS3 nup170-GFP:URA3</i>	original isolate from screen
SWY2335	<i>MATα npa12 lys2 ura3-1 his3-11,15 leu2-3,112 can1-100 ade2-1::ADE2:ura3 GFP-nic96:HIS3 nup170-GFP:URA3</i>	original isolate from screen
SWY2336	<i>MATα npa67 lys2 ura3-1 his3-11,15 leu2-3,112 can1-100 ade2-1::ADE2:ura3 GFP-nic96:HIS3 nup170-GFP:URA3</i>	original isolate from screen
YCH128	<i>MATα lys2 ura3-1 leu2-3,112 his3-11,15 ade2-1 ade3</i>	C. Hardy
ANY27	<i>MATα sar1::URA3 ura3 trp1 leu2 his3 his4 p[GAL1-SAR1 LEU2]</i>	Yamanushi et al., 1996
NY17	<i>MATα ura3-52 sec6-4</i>	Potenza et al., 1992
CKY39	<i>MATα ura3-52 his4-619 sec12-4</i>	Kurihara et al., 2000
CKY496	<i>MATα ura3-52 leu2-3,112 sec24-1</i>	Kurihara et al., 2000
RSY268	<i>MATα ura3-52 sec16-2</i>	Kaiser and Schekman, 1990
RSY1004	<i>MATα ura3-52 leu2-3,112 sec31-1</i>	Salama et al., 1997

Connections between Sec13p and NPC function have been previously reported. A fraction of the total cellular Sec13p is isolated in a NPC subcomplex containing Nup84p, Nup85p, Nup120p, Nup145p-C, and Seh1p (a Sec13-related protein) [40,41]. Hurt and coworkers have also reported that *ts sec13* mutants show enhanced growth

defects when combined with a *nup85 Δ* mutant, and result in the mislocalization of GFP-Nup49p to NE clusters and cytoplasmic foci [41]. This correlates with our observations of GFP-Nic96p and Nup170p-GFP in our *sec13/npa2* mutant. However, we did not observe clusters of herniated NPCs in *sec13-G176R/npa2-1* cells suggesting the *sec13-*

14 and *sec13-34* alleles in the Hurt study are distinct [41]. Precisely how Sec13p influences NPC structure/function remains to be elucidated.

The phenotypes observed in *sec13* and *sec23* mutants might indicate that COPII vesicles and/or a vesicular biogenesis step is required for NPC formation; however, there are at least two indirect mechanisms by which NPC structure may be changed in these mutants. Blocking the ER/Golgi pathway could titrate away the pool of Sec13p that is found at the NPC. Alternatively, the extensive ER proliferations that result are connected to the outer NE and could prevent proper NPC localization. Given that the formation of the extensive membrane networks in the *sec13* and *sec23* mutants was coincident with the GFP-Nup mislocalization, we favor one of the two indirect models. We feel this conclusion is also supported by our observation that the distribution of GFP-Nups was altered in mutants for all COPII coat components. However, not all of the COPII components co-fractionate with NPCs [5,6,42]. Thus, there are COPII components that perturb GFP-Nup localization that do not co-fractionate with NPCs. We conclude there is no absolute correlation between localization of a COPII component at the NPC and its ability to disrupt NPC structure/function. Instead, it is the *sec* mutants that alter ER structure that effect Nup localization.

The defects that we have observed in GFP-Nup localization in various *sec* mutants are distinct from recent reports characterizing a novel arrest of secretion response in *S. cerevisiae* cells. Tartakoff and coworkers have proposed that mutants with a secretory block show altered nuclear transport capacities, changes in the nuclear localization of particular proteins, and potential perturbations of NPC composition [60,61]. In our *sec13* and *sec23* mutants, we do not believe NPC composition has changed but rather that NPC localization has been altered by formation of extended ER networks.

Conclusions

Taken together, the work to date supports a framework wherein a network of in vivo interactions mediate NPC biogenesis, structural integrity, and proper localization in the NE. A complete understanding of the role of the NPC in nuclear transport will require the identification of all the genes that regulate its assembly, stability, and localization. Although the *npa/sec* mutants characterized here are due to ER distortions, we predict that further analysis of the other *npa* mutants and GFP-based genetic strategies will significantly contribute to the effort of identifying factors required for NPC biogenesis.

Methods

Yeast Strains

All yeast strains used in this study are listed in Table 1. General yeast manipulations were conducted by standard methods [62] with transformations by the lithium acetate method [63]. All strains were grown at 23° in YPD (yeast extract, peptone, 2% glucose) unless otherwise noted. The sequence encoding GFP was fused in frame to the 3' end of the *NUP170* open reading frame using the method of Baudin et al. [64]. To create a template for the polymerase chain reaction (PCR), the BamHI fragment of GFP S65T F64L [65] was first cloned into pRS316 [66]. The DNA fragment for integration was generated by PCR using the following oligonucleotides: Nup170G (5'-GATCCAATTGAAAAGTACGTTAAGAAGCAGCGGCAATAATTTGGGGATTITGTTTCTACAAAAGAAGCTGCGATGAG-TAAAGGAGAAGAAGCTT-3') and Nup170V (5'-TTACTTACAGATTACGATCTGTTCATGCATCAGAAATAGGAAGAAATTCAAAGCGGCATCAGAGCAGATTGT-3'). The resulting fragment was gel purified and transformed into SWY519. Correct chromosomal integration was confirmed by fluorescence microscopy and immunoblotting with anti-GFP antibodies (rabbit affinity purified IgG; kindly provided by M. Linder, Washington University School of Medicine, St. Louis, MO).

Crossing a *nup170-GFP:URA3* haploid isolate to SWY1695 generated doubly tagged *GFP-nic96 nup170-GFP* parental strains. The *lys2* marker was introduced by crossing to YCH128. GFP-tagged strains of other known mutants were made by crossing to either parental strain SWY2089 or SWY2090.

Null (Δ) deletion strains of *SEC13* and *SEC23* were purchased as heterozygous diploids from Research Genetics (Huntsville, AL). Each strain was transformed with a plasmid harboring the respective wild type gene in pRS316 (pSW1268 or pSW1269; see below) [66] and sporulated to isolate haploid *sec Δ* deletion strains with the pSEC/*URA3/CEN* plasmid. To test the function of the isolated mutant alleles, the resulting haploid *sec Δ* pSEC/*URA3/CEN* strains were transformed with the mutant *sec* alleles in a *LEU2/CEN* plasmid (pSW1264 or pSW1266; see below). Strains lacking the wild type *SEC/URA3/CEN* plasmids were isolated by growth on media containing 5-fluoroorotic acid (5-FOA).

Plasmids

Plasmids with wild type *SEC13* were generated with the following oligonucleotides (5' oligo *sec13N5* with 5'-CCCGGGCTAGCACTTCAATGTT-3'; 3' oligo *sec13-3* with 5'-ACCATTGAGCTCTTCACTGATGAAGTTCACC-3') using PCR and an isolated library plasmid as template. The PCR product was digested with SacI and XbaI and cloned into the SacI/XbaI sites of both pRS315 (pSW1264) and

pRS316 (pSW1268) [66]. Plasmids with wild type *SEC23* were constructed in the same manner using specific oligonucleotides (5' oligo *sec23F5* with 5'-ATGAATATCTA-GACCAGGTGCC-3'; 3' oligo *sec23-3* with 5'CCTTGATCCGTAGTAAAGGCCACGCAG-3') and digestion of the PCR product with XbaI and BamHI to yield pSEC23/*LEU2* (pSW1266) and pSEC23/*URA3* (pSW1269). Sequence for the mutant *sec13* and *sec23* alleles were cloned using the same oligonucleotide pairs with genomic DNA from SWY2324 or SWY2325, serving as template. Two independent PCR trials were completed for each mutant allele and cloned into the pRS315 vector [66]. Clones from each were obtained and both strands sequenced.

Mutagenesis and screening for mutants

Mutagenesis of SWY2089 and SWY2090 with ethylmethane sulfonate (EMS; Sigma, St. Louis, MO) was performed as described with the following modifications [67]. First, cells were mutagenized for 60, 75, and 90 minutes, followed by plating a fraction of the culture to determine cell viability at 23°. The remaining cells were stored in water at 4° for three days until the viability could be analyzed. The remaining mutagenized cell cultures were then plated to obtain ~100,000 colonies from each strain. To achieve this number, we assumed that roughly half of the cells died during the 4° storage. Temperature sensitive mutants were isolated by replica plating the master to both 23° and 34°, and screening for those that failed to grow at 34°. To screen for GFP-Nup localization, temperature sensitive strains were inoculated individually in 2 ml liquid YPD cultures and grown at 23° for 12–16 hours before shifting to 34° for 4–6 hours. The majority of the strains were in logarithmic growth phase at the time of the temperature shift. GFP localization was determined by direct fluorescence microscopy of unfixed cells. Fluorescence screening was repeated two additional times on those with an altered GFP pattern to confirm the phenotype.

Mutant complementation analysis

Complementation analysis of the temperature sensitive phenotypes was performed by crossing all the *MAT α* mutant strains to all *MAT α* mutant strains and selecting for diploids on media lacking lysine and tryptophan. Diploids were then replica plated back to YPD and assayed for growth at 34°. For direct testing, temperature sensitive mutants in genes involved in vesicular budding from the endoplasmic reticulum were obtained from others and crossed to all mutants isolated in the screen. Diploids were selected on appropriate minimal media, and then assayed for growth at the non-permissive temperature of 37°. (The GFP-Nups did not cause a temperature sensitive phenotype in heterozygous diploids). Additionally, the *sar1 Δ* crosses were grown on glucose to repress the plasmid borne copy of *GAL-SAR1*.

Microscopy

Live cell fluorescence and DIC microscopy was performed on an Olympus BX50 microscope using an UPlan 100X/1.3 objective. Cells for photography were grown in media lacking histidine, as the *HIS3* linked GFP-tag of *GFP-nic96* showed some instability in the *nup170-GFP* background. Images were captured using a Dage-MTI CCD-300-RC camera with NIH Image 1.61 or a Photometrics CoolSnap HQ camera with MetaVue software. Indirect immunofluorescence was performed as previously described [46]. Rabbit anti-Kar2 polyclonal antibodies [45] were used at 1:5000 and detected with Texas Red Goat-anti-Rabbit secondary antibody. The monoclonal mAb414 [68] and anti-Pom152 monoclonal mAb118C3 [69] were detected with FITC Goat-anti-mouse secondary. Thin section electron microscopy was conducted according to [36].

Molecular cloning

Selected mutants were backcrossed until the temperature sensitive phenotype segregated 2:2 and was shown to be linked to the GFP mislocalization phenotype. Identification of the mutant genes was accomplished by complementation of the temperature sensitive phenotype. The SWY2324, SWY2325, SWY2332, and SWY2333 strains were transformed with a *LEU2/CEN* yeast genomic library (ATCC, Manassas, VA). Transformants were grown for 48 hours at 23° and then shifted at 34°. Multiple overlapping inserts capable of rescuing the temperature sensitive growth defect were isolated for each strain. Sequencing of the insert ends and comparison to the *S. cerevisiae* Genome Database identified a region on chromosome XVI for *npa1-1* and *npa1-2* and chromosome XII for *npa2-1*. Plasmids expressing only *SEC23* or *SEC13* were used to test if these genes were necessary and sufficient for rescuing the phenotypes. Library inserts rescuing *npa3-1* contained a region of chromosome VII encompassing *SEC27*. A partial deletion of *SEC27* from one of the inserts (pSW1386) was used to confirm that *SEC27* was responsible for rescue of the growth defect. The temperature sensitive growth defect of *npa10* was rescued by a region on chromosome XI from YKR064W to the 5' end of *MET1*. The only essential gene in this region is *BET3*.

Invertase Assays

Mutants were grown at 23° overnight in 5 ml YPD to logarithmic phase. The equivalent of 1 ml of a 0.5 OD₆₀₀ cell culture was washed into YP media containing 0.05% glucose and incubated at 34° for 2.5 hours. The incubation was ended by addition of an equal volume of 20 mM sodium azide. Cell pellets were washed once with 10 mM sodium azide then resuspended in 800 μ l of 10 mM sodium azide. Assays of invertase activity were performed with 25 μ l of each sample according to [70,71]. The activity of each mutant was normalized to the activity of the parental strain assayed at the same time.

Acknowledgements

We wish to thank C. Hardy, C. Kaiser, A. Nakano, P. Novik, and R. Schekman for yeast strains; M. Rose for anti-Kar2 antibodies; M. Rout, C. Strambio-de-Castillia and G. Blobel for the anti-Pom152p monoclonal; A. Nett for help with cloning, and members of the Wentte lab for critical discussion. This work is supported by funds from the National Institutes of Health (GM20308 to K.J.R., and R01 GM57438 to S.R.W).

References

- Rout MP, Aitchison JD: **The nuclear pore complex as a transport machine.** *J Biol Chem* 2001, **276**:16593-16596
- Ryan KJ, Wentte SR: **The nuclear pore complex: a protein machine bridging the nucleus and cytoplasm.** *Curr Opin Cell Biol* 2000, **12**:361-371
- Stoffler D, Fahrenkrog B, Aebi U: **The nuclear pore complex: from molecular architecture to functional dynamics.** *Curr Opin Cell Biol* 1999, **11**:391-401
- Yang Q, Rout MP, Akey CW: **Three-dimensional architecture of the isolated yeast nuclear pore complex – functional and evolutionary implications.** *Mol Cell* 1998, **1**:223-234
- Rout MP, Aitchison JD, Suprpto A, Hjertaas K, Zhao Y, Chait BT: **The yeast nuclear pore complex: composition, architecture, and transport mechanism.** *J Cell Biol* 2000, **148**:635-651
- Cronshaw JM, Krutchinsky AN, Zhang W, Chait BT, Matunis MJ: **Proteomic analysis of the mammalian nuclear pore complex.** *J Cell Biol* 2002, **158**:
- Fontoura BMA, Blobel G, Matunis MJ: **A conserved biogenesis pathway for nucleoporins: proteolytic processing of a 186-kilodalton precursor generates Nup98 and the novel nucleoporin, Nup96.** *J Cell Biol* 1999, **144**:1097-1112
- Miller BR, Forbes DJ: **Purification of the vertebrate nuclear pore complex by biochemical criteria.** *Traffic* 2000, **1**:941-951
- Wentte SR: **Gatekeepers of the nucleus.** *Science* 2000, **288**:1374-1377
- Winey M, Yasar D, Giddings TH Jr, Mastonarde DN: **Nuclear pore complex number and distribution throughout the *Saccharomyces cerevisiae* cell cycle by three-dimensional reconstruction from electron micrographs of nuclear envelopes.** *Mol Biol Cell* 1997, **8**:2119-2132
- Gant TM, Wilson KL: **Nuclear Assembly.** *Annu Rev Cell Dev Biol* 1997, **13**:669-695
- Bodoor K, Shaikh S, Salina D, Raharjo WJ, Bastos R, Lohka M, Burke B: **Sequential recruitment of NPC proteins to the nuclear periphery at the end of mitosis.** *J Cell Sci* 1999, **112**:2253-2264
- Haraguchi T, Koujin T, Hayakawa T, Kaneda T, Tsutsumi C, Imamoto N, Akazawa C, Sukegawa J, Yoneda Y, Hiraoka Y: **Live fluorescence imaging reveals early recruitment of emerin, LBR, RanBP2, and Nup153 to reforming functional nuclear envelopes.** *J Cell Sci* 2000, **113**:779-794
- Daigle N, Beaudouin J, Hartnell L, Imreh G, Hallberg E, Lippincott-Schwartz J, Ellenberg J: **Nuclear pore complexes form immobile networks and have very low turnover in live mammalian cells.** *J Cell Biol* 2001, **154**:71-84
- Belgareh N, Rabut G, Bai SW, van Overbeek M, Beaudouin J, Daigle N, Zatschina OV, Pasteau F, Labas V, M Fromont-Racine, et al: **An evolutionarily conserved NPC subcomplex, which redistributes in part to kinetochores in mammalian cells.** *J Cell Biol* 2001, **154**:1147-1160
- Macaulay C, Forbes DJ: **Assembly of the nuclear pore – biochemically distinct steps revealed with NEM, GTP-gamma-S, and BAPTA.** *J Cell Biol* 1996, **132**:5-20
- Goldberg MW, Wiese C, Allen TD, Wilson KL: **Dimples, pores, star-rings, and thin rings on growing nuclear envelopes: evidence for structural intermediates in nuclear pore complex assembly.** *J Cell Sci* 1997, **110**:409-420
- Smythe C, Jenkins HE, Hutchison CJ: **Incorporation of the nuclear pore basket protein Nup153 into nuclear pore structures is dependent upon lamina assembly: evidence from cell-free extracts of *Xenopus* eggs.** *EMBO J* 2000, **19**:3918-3931
- Walther TC, Fornerod M, Pickersgill H, Goldberg M, Allen TD, Mattaj JW: **The nucleoporin Nup153 is required for nuclear basket formation, nuclear pore complex anchoring and import of a subset of nuclear proteins.** *EMBO J* 2001, **20**:5703-5714
- Lutzmann M, Kunze R, Buerer A, Aebi U, Hurt E: **Modular self-assembly of a Y-shaped multiprotein complex from seven nucleoporins.** *EMBO J* 2002, **21**:387-397
- Wentte SR, Gasser SM, Caplan AJ: **The nucleus and nucleocytoplasmic transport in *Saccharomyces cerevisiae*.** In: *The Molecular and Cellular Biology of the Yeast *Saccharomyces** (Edited by: JR Broach, E Jones, J Pringle) Cold Spring Harbor, New York: Cold Spring Harbor Laboratory Press; 1997, **3**:471-546
- Doye V, Hurt E: **From nucleoporins to nuclear pore complexes.** *Curr Opin Cell Biol* 1997, **9**:401-411
- Gomez-Ospina N, G Morgan, Giddings J, T. H., Kosova B, Hurt E, Winey M: **Yeast nuclear pore complex assembly defects determined by nuclear envelope reconstruction.** *J Struct Biol* 2000, **132**:1-5
- Marelli M, Lusk CP, Chan H, Aitchison JD, Wozniak RW: **A link between the synthesis of nucleoporins and the biogenesis of the nuclear envelope.** *J Cell Biol* 2001, **153**:709-723
- Bucci M, Wentte SR: **In vivo dynamics of nuclear pore complexes in yeast.** *J Cell Biol* 1997, **136**:1185-1199
- Bucci M, Wentte SR: **A novel fluorescence-based genetic strategy identifies mutants of *Saccharomyces cerevisiae* defective for nuclear pore complex assembly.** *Mol Biol Cell* 1998, **9**:2439-2461
- Grandi P, Schlaich N, Tekotte H, Hurt EC: **Functional interaction of Nic96p with a core nucleoporin complex consisting of Nsp1p, Nup49p and a novel protein Nup57p.** *EMBO J* 1995, **14**:76-87
- Schlaich NL, Haner M, Lustig A, Aebi U, Hurt EC: **In vitro reconstitution of a heterotrimeric nucleoporin complex consisting of recombinant Nsp1p, Nup49p, and Nup57p.** *Mol Biol Cell* 1997, **8**:33-46
- Grandi P, Doye V, Hurt EC: **Purification of NSP1 reveals complex formation with 'GLFG' nucleoporins and a novel nuclear pore protein NIC96.** *EMBO J* 1993, **12**:3061-71
- Kosova B, Pante N, Rollenhagen C, Hurt E: **Nup192p is a conserved nucleoporin with a preferential location at the inner side of the nuclear membrane.** *J Biol Chem* 1999, **274**:22646-22651
- Aitchison JD, Rout MP, Marelli M, Blobel G, Wozniak RW: **Two novel related yeast nucleoporins Nup170p and Nup157p – complementation with the vertebrate homologue Nup155p and functional interactions with the yeast nuclear pore-membrane protein Pom152p.** *J Cell Biol* 1995, **131**:1133-1148
- Kenna MA, Petranka JG, Reilly JL, Davis LI: **Yeast N1e3p/Nup170p is required for normal stoichiometry of FG nucleoporins within the nuclear pore complex.** *Mol Cell Biol* 1996, **16**:2025-2036
- Marelli M, Aitchison JD, Wozniak RW: **Specific binding of the karyopherin Kap121p to a subunit of the nuclear pore complex containing Nup53p, Nup59p, and Nup170p.** *J Cell Biol* 1998, **143**:1813-1830
- Tcheperegine SE, Marelli M, Wozniak RW: **Topology and functional domains of the yeast pore membrane protein Pom152p.** *J Biol Chem* 1999, **274**:5252-5258
- Zabel U, Doye V, Tekotte H, Wepf R, Grandi P, Hurt EC: **Nic96p is required for nuclear pore formation and functionally interacts with a novel nucleoporin, Nup188p.** *J Cell Biol* 1996, **133**:1141-1152
- Wentte SR, Blobel G: **A temperature-sensitive NUP116 null mutant forms a nuclear envelope seal over the yeast nuclear pore complex thereby blocking nucleocytoplasmic traffic.** *J Cell Biol* 1993, **123**:275-84
- Novick P, Field C, Schekman R: **Identification of 23 complementation groups required for post-translational events in the yeast secretory pathway.** *Cell* 1980, **21**:205-215
- Barlowe C, Orci L, Yeung T, Hosobuchi M, Hamamoto S, Salama NR, Rexach MF, Ravazzola M, Amherdt M, Schekman R: **COPII: a membrane coat formed by Sec proteins that drive vesicle budding from the endoplasmic reticulum.** *Cell* 1994, **77**:895-907
- Kaiser CA, Ferro-Novick S: **Transport from the endoplasmic reticulum to the Golgi.** *Curr Opin Cell Biol* 1998, **10**:477-482
- Siniossoglou S, Wimmer C, Rieger M, Doye V, Tekotte H, Weise C, Emig S, Segref A, Hurt EC: **A novel complex of nucleoporins, which includes Sec13p and a Sec13p homologue, is essential for normal nuclear pores.** *Cell* 1996, **84**:265-275

41. Siniouoglou S, Lutzmann M, Santos-Rosa H, Leonard K, Mueller S, Aebi U, Hurt E: **Structure and assembly of the Nup84p complex.** *J Cell Biol* 2000, **149**:41-53
42. Allen NPC, Huang L, Burlingame A, Rexach M: **Proteomic analysis of nucleoporin interacting proteins.** *J Biol Chem* 2001, **276**:29268-29274
43. Yoshihisa T, Barlowe C, Schekman R: **Requirement for a GTPase-activating protein in vesicle budding from the endoplasmic reticulum.** *Science* 1993, **259**:1466-1468
44. Kaiser CA, Schekman R: **Distinct sets of SEC genes govern transport vesicle formation and fusion early in the secretory pathway.** *Cell* 1990, **61**:723-733
45. Rose MD, Misra LM, Vogel JP: **KAR2, a karyogamy gene, is the yeast homolog of the mammalian BiP/GRP78 gene.** *Cell* 1989, **57**:1211-1221
46. Wente SR, Rout MP, Blobel G: **A new family of yeast nuclear pore complex proteins.** *J Cell Biol* 1992, **119**:705-723
47. Sacher M, Jiang Y, Barrowman J, Scarpa A, Burston J, Zhang L, Schieltz D, Yates JRI, Abeliovich H, S Ferro-Novick: **TRAPP, a highly conserved novel complex on the cis-Golgi that mediates docking and fusion.** *EMBO J* 1998, **17**:2494-2503
48. Sacher M, Barrowman J, Wang W, Horecka J, Pypaert M, Ferro-Novick S: **TRAPP I implicated in the specificity of tethering in ER-to Golgi transport.** *Mol Cell* 2001, **7**:433-442
49. Duden R, Hosobuchi M, Hamamoto S, Winey M, Byers B, Schekman R: **Yeast β - and β' - coat proteins (COP).** *J Biol Chem* 1994, **269**:24486-24495
50. Barlowe C: **Traffic COPs of the early secretory pathway.** *Traffic* 2000, **1**:371-377
51. Rossi G, Kolstad K, Stone S, Palluault F, Ferro-Novick S: **BET3 encodes a novel hydrophilic protein that acts in conjunction with yeast SNAREs.** *Mol Biol Cell* 1995, **6**:1769-1780
52. Potenza M, Bowser R, Muller H, Novick P: **SEC6 encodes an 85 kDa protein required for exocytosis in yeast.** *Yeast* 1992, **8**:549-558
53. Letourneur F, Gaynor EC, Hennecke S, Demolliere C, Duden R, Emr SD, Riezman H, Cosson P: **Coatamer is essential for retrieval of dilysine-tagged proteins to the endoplasmic reticulum.** *Cell* 1994, **79**:1199-1207
54. Trumbly RJ: **Glucose repression in the yeast *Saccharomyces cerevisiae*.** *Mol Microbiol* 1992, **6**:15-21
55. Matynia A, Salus SS, Sazer S: **Three proteins required for early steps in the secretory pathway also affect nuclear envelope structure and cell cycle progression in fission yeast.** *J Cell Sci* 2002, **115**:421-431
56. Yamanushi T, Hirata A, Oka T, Nakano A: **Characterization of yeast *sarl* temperature-sensitive mutants, which are defective in protein transport from the endoplasmic reticulum.** *J Biochem* 1996, **120**:452-458
57. Wuestehube LJ, Duden R, Eun A, Hamamoto S, Korn P, Ram R, Schekman R: **New mutants of *Saccharomyces cerevisiae* affected in the transport of proteins from the endoplasmic reticulum to the Golgi complex.** *Genetics* 1996, **142**:393-406
58. Kurihara T, Hamamoto S, Gimeno RE, Kaiser CA, Schekman R, Yoshihisa T: **Sec24p and Issl1p function interchangeably in transport vesicle formation from the endoplasmic reticulum in *Saccharomyces cerevisiae*.** *Mol Biol Cell* 2000, **11**:983-998
59. Higashio H, Kimata Y, Kiriya T, Hirata A, Kohno K: **Sfb2, a yeast protein related to Sec24p, can function as a constituent of COPII coats required for vesicle budding from the endoplasmic reticulum.** *J Biol Chem* 2000, **275**:17900
60. Nanduri J, Mitra S, Andrei C, Liu Y, Yu Y, Hitomi M, Tartakoff AM: **An unexpected link between the secretory path and the organization of the nucleus.** *J Biol Chem* 1999, **274**:33785-33789
61. Nanduri J, Tartakoff AM: **The arrest of secretion response in yeast: signaling from the secretory path to the nucleus via Wsc proteins and Pkc1p.** *Mol Cell* 2001, **8**:281-289
62. Sherman F, Fink GR, Hicks JB: **Methods in Yeast Genetics.** Cold Spring Harbor, NY: Cold Spring Harbor Laboratory Press; 1986
63. Ito H, Fukuda Y, Murata K, Kimura A: **Transformation of intact yeast cells treated with alkali cations.** *J Bacteriol* 1983, **153**:163-168
64. Baudin A, Ozier KO, Denouel A, Lacroute F, Cullin C: **A simple and efficient method for direct gene deletion in *Saccharomyces cerevisiae*.** *Nucleic Acids Res* 1993, **21**:3329-3330
65. Heim R, Tsien RY: **Engineering green fluorescent protein for improved brightness, longer wavelengths and fluorescence resonance energy transfer.** *Curr Biol* 1996, **6**:178-182
66. Sikorski RS, Hieter P: **A system of shuttle vectors and yeast host strains designed for efficient manipulation of DNA in *Saccharomyces cerevisiae*.** *Genetics* 1989, **122**:19-27
67. Lawrence CW: **Classical mutagenesis techniques.** In: *Guide to yeast genetics and molecular biology* (Edited by: C Guthrie, GR Fink, vol) San Diego, CA: Academic Press, Inc 1991, **194**:273-280
68. Davis LI, Blobel G: **Identification and characterization of a nuclear pore complex protein.** *Cell* 1986, **45**:699-709
69. Strambio-de-Castillia C, Blobel G, Rout MP: **Isolation and characterization of nuclear envelopes from the yeast *Saccharomyces*.** *J Cell Biol* 1995, **131**:19-31
70. Goldstein A, Lampen JO: **β -D-fructofuranoside fructohydrolase from yeast.** *Methods Enzymol* 1975, **42C**:504-511
71. Hubbard EJ, Yang XL, Carlson M: **Relationship of the cAMP-dependent protein kinase pathway to the SNF1 protein and invertase expression in *Saccharomyces cerevisiae*.** *Genetics* 1992, **130**:71-80

Publish with **BioMed Central** and every scientist can read your work free of charge

"BioMedCentral will be the most significant development for disseminating the results of biomedical research in our lifetime."

Paul Nurse, Director-General, Imperial Cancer Research Fund

Publish with **BMC** and your research papers will be:

- available free of charge to the entire biomedical community
- peer reviewed and published immediately upon acceptance
- cited in PubMed and archived on PubMed Central
- yours - you keep the copyright



Submit your manuscript here:

<http://www.biomedcentral.com/manuscript/>

editorial@biomedcentral.com